Available online at www.sciencedirect.com
SCIENCE DIRECT®
Journal of the Mechanics and Physics of Solids
54 (2006) 783–806
JOURNAL OF THE MECHANICS AND PHYSICS OF SOLIDS
www.elsevier.com/locate/jmps

Effects of cell shape and strut cross-sectional area variations on the elastic properties of three-dimensional open-cell foams

K. Li[a], X.-L. Gao[a,*], G. Subhash[b]

[a]*Department of Mechanical Engineering, Texas A&M University, 3123 TAMU, College Station, TX 77843-3123, USA*
[b]*Department of Mechanical Engineering-Engineering Mechanics, Michigan Technological University, 1400 Townsend Drive, Houghton, MI 49931-1295, USA*

Received 12 February 2005; accepted 25 October 2005

Abstract

The Voronoi tessellation technique and the finite element (FE) method are utilized to investigate the microstructure–property relations of three-dimensional (3-D) cellular solids (foams) that have irregular cell shapes and non-uniform strut cross-sectional areas (SCSAs). Perturbations are introduced to a regular packing of seeds to generate a spatially periodic Voronoi diagram with different degrees of cell shape irregularity (amplitude a), and to the constant SCSA to generate a uniform distribution of SCSAs with different degrees of SCSA non-uniformity (amplitude b). Twenty FE models are constructed, based on the Voronoi diagrams for twenty foam samples (specimens) having the same pair of a and b, to obtain the mean values and standard deviations of the elastic properties. Spatially periodic boundary conditions are applied to each specimen. The simulation results indicate that for low-density imperfect foams, the elastic moduli increase as cell shapes become more irregular, but decrease as SCSAs get less uniform. When the relative density (R) increases, the elastic moduli of imperfect foams increase substantially, while the Poisson's ratios decrease moderately. The effect of the interaction between the two types of imperfections on foam elastic properties appears to be weak. In addition, it is found that the strut cross-sectional shape has a significant effect on the foam properties. Also, the elastic response of foams with the cell shape and

*Corresponding author. Tel.: +1 979 845 4835; fax: +1 979 845 3081.
E-mail address: xlgao@tamu.edu (X.-L. Gao).

0022-5096/$ - see front matter
doi:10.1016/j.jmps.2005.10.007

SCSA imperfections appears to be isotropic regardless of changes in a, b and R and the strut cross-sectional shape.

Keywords: Open-cell foams; Irregular cell shapes; Non-uniform strut cross-sectional areas; Voronoi tessellation; Structure–property relations

1. Introduction

Many models, analytical or experimental, have been developed, based on idealized unit cells, for predicting mechanical properties of cellular solids. A unit cell (also called repeating unit), when properly identified, can capture the essential microstructural features of an actual cellular material. For three-dimensional (3-D) cellular solids (foams), cubic, tetrahedral, dodecahedral and tetrakaidecahedral cells have been used as repeating units. A cubic cell based model for 3-D open-cell foams was developed by Gibson and Ashby (1997). More recent unit cell based models that lead to closed-form structure-property relations include those of Warren and Kraynik (1997), Zhu et al. (1997) and Li et al. (2003), all of which employed tetrakaidecahedral cells.

Although unit cell-based models can provide important results, they are significantly limited by their inability to account for microstructural imperfections inherent in most real cellular materials, whose cell structures are typically non-periodic, non-uniform and disordered (e.g., Matzke, 1946; Kraynik et al., 2003, 2004; Gong et al., 2005a). Thus, more complex, statistical models are needed to obtain improved predictions. To this end, suitable numerical methods are often required because of the stochastic nature of the problem.

Efforts have been made to explore the effects of imperfections, such as irregular cell shapes and sizes (Van der Burg et al., 1997; Bart-Smith et al., 1998; Grenestedt and Tanaka, 1999; Roberts and Garboczi, 2001, 2002; Zhou et al., 2002), thickness variations between cell walls (Grenestedt and Bassinet, 2000), non-uniform solid distribution in cell walls (Simone and Gibson, 1998a), curved/corrugated cell walls (Simone and Gibson, 1998b), and wavy cell walls (Grenestedt, 1998), on mechanical properties of 3-D open-cell and closed-cell foams. However, in each of these existing studies, only one type of imperfection was included at a time. In general, two or more types of imperfections are simultaneously involved in the microstructure of a cellular material. Therefore, models incorporating two or more types of imperfections are still needed.

The objective of this paper is to study the combined effects of two co-existing imperfections—irregular cell shapes and non-uniform strut cross-sectional areas (SCSAs)—on the elastic properties of 3-D open-cell foams. The rest of this paper is organized as follows. In Section 2, foams with different degrees of cell shape irregularity and SCSA non-uniformity are first constructed using the Voronoi tessellation technique. Twenty finite element (FE) models are then developed using the constructed Voronoi diagrams to calculate the effective Young's moduli, Poisson's ratios and shear moduli of the foams. Each of these diagrams (specimens) contains 125 Voronoi cells. The cell morphology of the random foam models is also analyzed in this section. In Section 3, a size sensitivity study is first performed to determine the appropriate number of cells to be included in each specimen and the suitable number of specimens to be used in statistical

analysis. This is followed by an investigation of the elastic behavior (isotropic or anisotropic) of the foams based on the Voronoi diagrams and FE models. Finally, a parametric study is conducted for sample cases involving various values of a, b and R, and different cross-sectional shapes. The paper concludes with a summary in the fourth section.

2. Analysis

Three-dimensional open-cell foams (e.g., graphitic carbon foams) are often produced through a bubble forming process. As a result, microstructures of such foams are controlled by the principle of minimum surface energy (Kraynik, 2003). This indicates that the morphology of such a 3-D open-cell foam may be best represented by packed tetrakaidecahedral cells [also called Kelvin cells after Lord Kelvin, Thompson (1887)], since tetrakaidecahedron is known to be the only polyhedron that can pack with identical units to fill space (see Fig. 1) and nearly minimize the surface energy (e.g., Weaire and Fortes, 1994).

Due to the similarity between the mathematical procedure of the Voronoi tessellation and the physics of foam production, the Voronoi tessellation technique is a natural choice for describing the microstructure of a foam resulting from a bubble forming process. The Voronoi tessellation of space is fully determined by the initial locations of generating seeds (e.g., Glaessgen et al., 2003). Using regularly positioned seeds produces regular Voronoi diagrams. The current analysis starts with a reference model, which is a tetrakaidecahedral (Kelvin) foam structure with cells of regular shapes and struts of uniform cross-sectional areas. This reference model is constructed from a set of regularly packed seeds sitting on a body-centered cubic (BCC) lattice using the Voronoi tessellation technique, as shown in Fig. 1. Perturbations are then introduced to the reference model to generate Voronoi

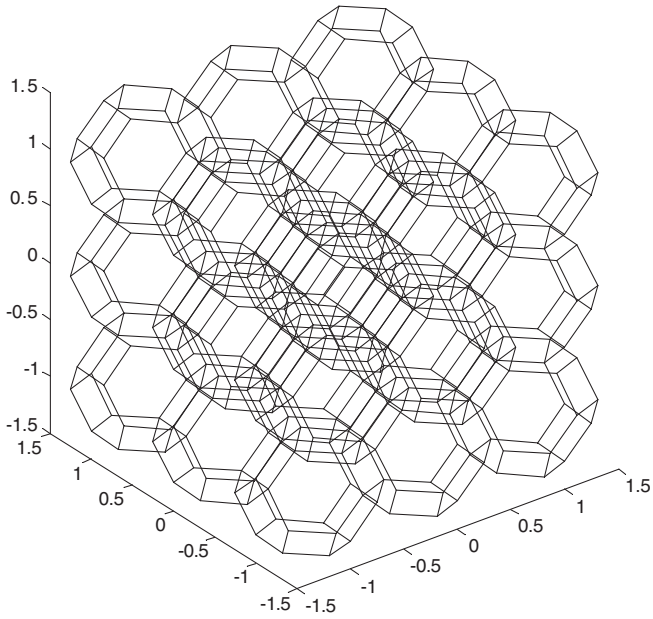

Fig. 1. A regular foam sample with 27 complete cells.

diagrams with irregular cell shapes and non-uniform SCSAs (e.g., Grenestedt and Tanaka, 1999; Grenestedt and Bassinet, 2000). The non-uniformity here and in the sequel means that the cross-sectional area of each strut may differ from that of any other strut, although each strut is regarded as having a constant cross-sectional area along its length and the cross-sectional shape remains the same for all the struts.

2.1. Spatially periodic random foams with cell shape and SCSA variations

To generate a spatially periodic random foam model, a set of seeds of periodic symmetry needs to be employed (e.g., Nygards and Gudmundson, 2002). To this end, a pre-set number of seeds are first generated within a parallelepiped having the desired dimensions. Then, the position of each seed within the parallelepiped is copied to 26 identical parallelepipeds adjacent to or sitting at the corners of the original parallelepiped. Finally, the Voronoi tessellation technique is applied to all of the seeds within the 27 parallelepipeds. Part of the resulting Voronoi tessellation that is inscribed by the central (original) parallelepiped can then be taken out as the periodic specimen of the specified size. In this study, the needed Voronoi diagrams are constructed using the program Qhull developed at the Geometry Center, the University of Minnesota–Twin Cities (now available at http://www.qhull.org/).

The irregularity of cell shapes is determined by the irregular distribution of the seeds. By perturbing the locations of the seeds sitting on a BCC lattice, the coordinates of a perturbed seed k can be obtained as (e.g., Grenestedt and Tanaka, 1999)

$$x_i^k = \bar{x}_i^k + aL\varphi_i^k, \tag{1}$$

where $\bar{x}_i^k$ ($i \in \{1,2,3\}$) are the coordinates of the same seed k in the initially regular lattice, L is the height of a regular tetrakaidecahedron, φ_i^k ($\in [-1,1]$) is a random variable with a uniform distribution, and a ($\in [0,1]$) is the amplitude used to quantify the degree of cell shape irregularity. The smaller a is, the more regular the Voronoi diagram is, as illustrated in Fig. 2. Regular 3-D foams are obtained when $a = 0$, and completely irregular foams are defined when $a = 1.0$. Fig. 2 shows foam samples with different degrees of cell shape irregularity. Each sample includes 125 complete Voronoi cells. It is noted from Fig. 2 that the two foam specimens with $a = 0.5$ and 1.0 respectively have very similar cell shapes. This is because when a is greater than 0.5, the cubic space reachable by a seed, whose coordinates are defined by Eq. (1), overlaps with those spaces reachable by its adjacent

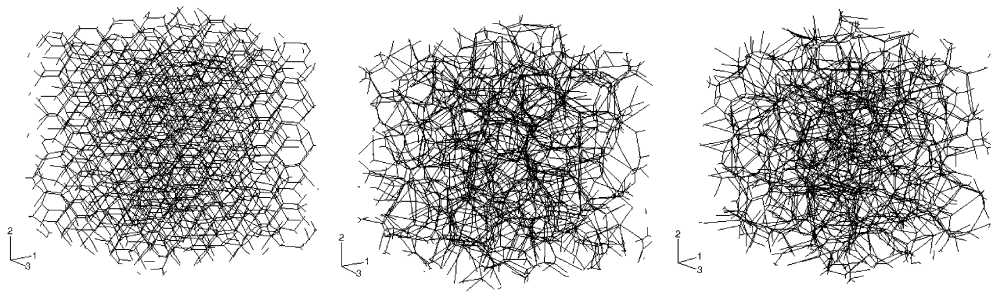

Fig. 2. Foam samples with varying a: (a) $a = 0.1$, (b) $a = 0.5$, (c) $a = 1.0$.

seeds, thereby leading to highly irregular cells in the resulting Voronoi diagram before a reaches 1.0. The cell morphology analysis to be presented in Section 2.2 supports the observation here.

As indicated in Eq. (1), for given relative density and amplitude of cell shape irregularity, the predicted properties of a foam having uniform SCSAs depend on the set of stochastic variables φ_i^k ($i \in \{1,2,3\}$; $k \in \{1,\ldots,M\}$, M = the total number of seeds). These variables are produced using a generator of uniform random numbers. To obtain the expectation values of the foam properties, a significant number of simulations with various sets of φ_i^k ($\in [-1,1]$) are needed. In this study, twenty samples are analyzed for each value of a. The choice of twenty specimens (samples) will be discussed further in Section 3.

After the cell shapes are determined, statistical variations of SCSAs can be introduced to the uniform SCSA, A_0, given by

$$A_0 = RL_1L_2L_3 \Big/ \sum_{j=1}^{N} l_j, \tag{2}$$

where R is the relative foam density, L_1, L_2 and L_3 are the dimensions of the foam sample (specimen), l_j is the length of strut j, and N is the total number of struts. To this end, each strut is assigned a random area given by (e.g., Grenestedt and Bassinet, 2000)

$$A_j = wA_0(1 + b\psi_j), \tag{3}$$

where b ($\in [0,1]$) is the amplitude used to quantify the degree of non-uniformity of SCSAs, ψ_j ($\in [-1,1]$) is a random variable with a uniform distribution, and w, called the normalizing factor, is defined by

$$w = \sum_{j=1}^{N} l_j \Big/ \left[\sum_{j=1}^{N}(1 + b\psi_j)l_j\right] \tag{4}$$

to ensure that the relative density remains unchanged with the variation of SCSAs. Given R, a, b and the set of random variables φ_i^k ($i \in \{1,2,3\}$; $k \in \{1,\ldots,M\}$), the predicted foam properties depend on the set of random variables ψ_j ($j \in \{1,2,\ldots,N\}$), which are generated independently of φ_i^k. Statistically, it is required to run sufficient simulations with different sets of ψ_j to get the expectation values of the foam properties. In this study, twenty foam samples, with a remaining fixed for each sample, will be analyzed for each given value of b. Similarly, twenty samples are considered for each value of a when b is held constant, as indicated earlier. The reason for choosing twenty specimens will be provided in Section 3.

2.2. Cell morphology

The cell morphology of the random foam models constructed by following the procedure described above in Section 2.1 is analyzed here to explore the cell structural features, including number of faces per polyhedral cell (f) and number of edges per polygonal face (n). Each foam specimen considered contains 125 cells. In a perfectly ordered Kelvin foam ($a = 0$) specimen, there are 125 complete tetrakaidecahedral cells, each of which contains six identical squares and eight identical hexagons. The cell shapes are irregular for foam specimens with $a \neq 0$. However, the total number of cells (Voronoi rather than tetrakaidecahedral cells) remains to be 125 in such a random foam specimen, since the specimen is cut out of a spatially periodic Voronoi diagram using a bounding

parallelepiped that has the same dimensions as the spatial periods of the Voronoi diagram. An incomplete cell on one boundary face can always find its remaining part on the opposite boundary face of the specimen to form a complete Voronoi cell.

The distributions of f and n are shown in Figs. 3 and 4, where $p(f)$ and $p(n)$ are, respectively, the probabilities of having f faces in each cell and n edges in each face. It is seen from these figures that as a increases, both $p(f)$ and $p(n)$ spectra broaden, and the peak value of $p(f)$ shifts toward higher f, while that of $p(n)$ shifts toward lower n. The average number of faces per cell, $\langle f \rangle$, and the average number of edges per face, $\langle n \rangle$, which is obtained using the formula $\langle n \rangle = 6 - 12/\langle f \rangle$ available for spatially periodic 3-D foams (e.g., Kraynik et al., 2003), are shown in Figs. 5 and 6, respectively. The mean value and standard deviation are calculated based on twenty specimens for each value of a except

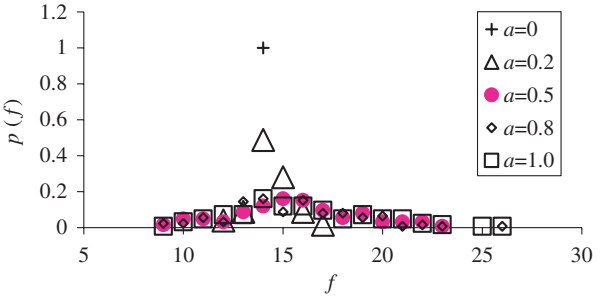

Fig. 3. Distribution of number of faces per polyhedral cell.

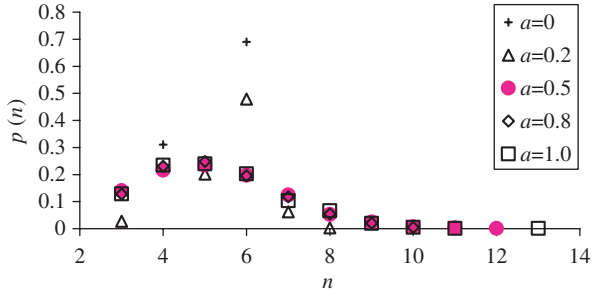

Fig. 4. Distribution of number of edges per polygonal face.

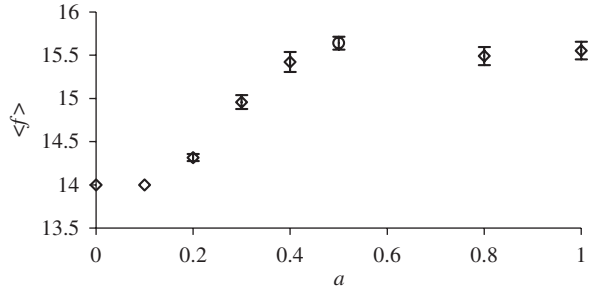

Fig. 5. Average number of faces per polyhedral cell.

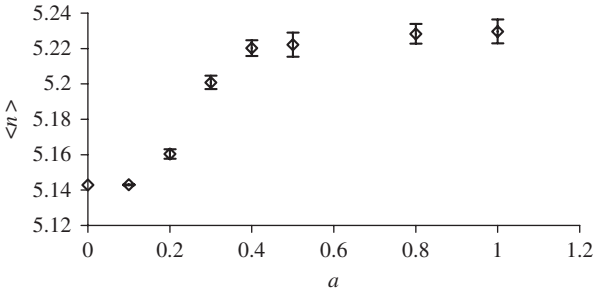

Fig. 6. Average number of edges per polygonal face.

for the case with $a = 0$ (i.e., the perfectly ordered Kelvin foam), where only one specimen is used. From Figs. 5 and 6, it is observed that the Kelvin foam (with $a = 0$) has the minimum values of $\langle f \rangle$ ($= 14$) and $\langle n \rangle$ ($= 5.143$). As a increases (up to $a = 0.5$), both $\langle f \rangle$ and $\langle n \rangle$ increase. A further increase of a (beyond 0.5) does not lead to significant changes in $\langle f \rangle$ and $\langle n \rangle$. This verifies and supports the observation made earlier based on Fig. 2.

2.3. Finite element analysis

A finite element study is performed to obtain the elastic properties of foams with cell shape and SCSA irregularities using the commercial software package ABAQUS 6.3 (Hibbitt et al., Inc., 2002, Pawtucket, RI). Graphitic carbon foams are considered here. The Young's modulus E_s and Poisson's ratio v_s of the carbon strut material are, respectively, taken to be 15.61 GPa and 0.33 (Li et al., 2003, 2005a). Each strut is represented using a three-node beam element (element type B32 in ABAQUS), which involves bending, stretching, twisting and shearing deformation mechanisms. A preliminary study has shown that using such a beam element to model each strut is sufficient for convergence. It is noted that exceptionally short struts do exist in foam specimens having highly irregular cell shapes. Typical beam elements cannot represent these short struts well. However, since short struts only account for a small fraction (a few percent) of the total number of struts, the effect incurred from using inappropriate element types is negligible (Van der Burg et al., 1997).

Uniaxial compressive tests on foam specimens along three orthogonal directions, x_1, x_2 and x_3, are considered in three separate analyses to obtain the effective Young's moduli and Poisson's ratios of the foam relative to the three directions. In each analysis, a small compressive strain (e.g., -0.001) is applied in the loading direction such that no local buckling of struts will take place. The effective Young's modulus, E_1, and Poisson's ratios, ν_{12} and ν_{13}, of the foam along the x_1 direction are given by

$$E_1 = \frac{-F_1}{\varepsilon_1 L_2 L_3}, \tag{5}$$

$$\nu_{12} = -\frac{u_2^1}{\varepsilon_1 L_2}, \quad \nu_{13} = -\frac{u_3^1}{\varepsilon_1 L_3}, \tag{6a,b}$$

where ε_1 ($= -0.001$) is the applied compressive strain, and F_1 is the total reaction force along x_1 direction on the prescribed boundary, which is to be obtained from the finite element analysis, and u_j^i ($i,j \in \{1,2,3\}$) is the lateral displacement (extension) in the x_j direction perpendicular to the loading direction x_i. The effective Young's moduli and Poisson's ratios along the x_2 and x_3 directions, E_2, E_3, ν_{21}, ν_{23}, ν_{31} and ν_{32}, can be similarly determined.

To obtain the effective shear modulus G_{12}, a biaxial loading test is simulated. A tensile strain $\varepsilon_1 = 0.001$ in the x_1 direction and a compressive strain $\varepsilon_2 = -0.001$ in the x_2 direction are applied simultaneously. Then, the effective shear modulus G_{12}, defined by $G_{12} = \tau_{12}/\gamma_{12}$, is given by

$$G_{12} = \frac{F_1/L_2 - F_2/L_1}{2L_3(\varepsilon_1 - \varepsilon_2)}. \tag{7}$$

The other two shear moduli, G_{23} and G_{31}, can be similarly determined.

In modeling uniaxial or biaxial loading tests, displacement boundary conditions are typically used (e.g., Silva et al., 1995; Silva and Gibson, 1997; Van der Burg et al., 1997; Simone and Gibson, 1998a, b). However, displacement boundary conditions that only restrain normal displacements may underestimate foam properties (e.g., Li et al., 2005b). Since the specimen is cut out of an infinite structure that can be regarded as periodic, spatially periodic boundary conditions should be applied to ensure that the predicted properties of the specimen are representative of those of the foam material (Laroussi et al., 2002; Roberts and Garboczi, 2002; Li et al., 2005b). The specimen obtained by following the procedure described in Section 2.1 is periodic, i.e., each node on one face (e.g., v^-) has a matched node on the opposite face of the specimen (e.g., v^+), as shown in Fig. 7. For a uniaxially deformed specimen subjected to prescribed strain ε_i, the periodic boundary conditions may be represented by

$$u_i^{k^+} - u_i^{k^-} = \varepsilon_i(x_i^{k^+} - x_i^{k^-}), \quad \omega_i^{k^+} - \omega_i^{k^-} = 0, \quad i \in \{1,2,3\}, \tag{8}$$

where $x_i^{k^+}$ and $x_i^{k^-}$ are, respectively, the positions of the matched nodes k^+ and k^- on the specimen boundary faces with outward unit normal vectors $\boldsymbol{e}_i$ and $-\boldsymbol{e}_i$, $u_i^{k^+}$ and $u_i^{k^-}$ are, respectively, the normal displacement components of k^+ and k^-, and ω_i^+ and ω_i^- are,

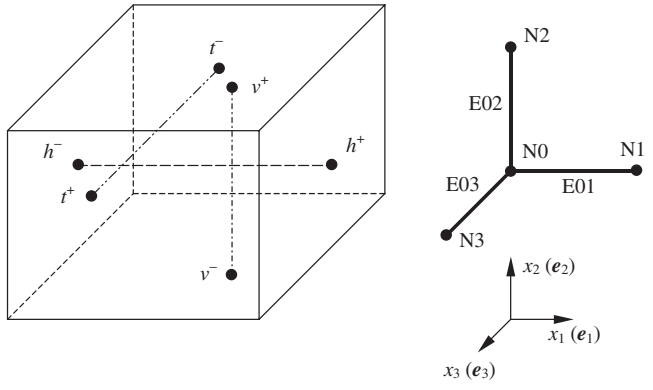

Fig. 7. Matched nodes for implementing spatially periodic boundary conditions.

respectively, the rotations of k^+ and k^-. It should be noted that the periodic boundary conditions defined by Eq. (8) work well only for foams undergoing small deformations, which is the case here (with the applied compressive strain taken to be $\varepsilon_i = -0.001$ in using Eqs. (5)–(7)). When foams are subjected to large compressive strains, however, non-periodic localized deformations may occur (e.g., Gong et al., 2005b) and periodic boundary conditions can no longer be adequately applied.

The periodic boundary conditions given in Eq. (8) can be implemented by using the option EQUATION in ABAQUS and by introducing four reference nodes N0, N1, N2 and N3, which define three two-node AXIAL connector elements E01, E02 and E03 (see Fig. 7). The three connector elements intersect at reference node N0 and are located along the $\boldsymbol{e}_1$, $\boldsymbol{e}_2$ and $\boldsymbol{e}_3$ directions, respectively. Nodes N1, N2 and N3 are allowed to move axially only along their associated connector elements. The degrees of freedom of the matched nodes may be coupled with those of the reference nodes by

$$u_i^{k^+} - u_i^{k^-} - \frac{x_i^{k^+} - x_i^{k^-}}{X_i^{K^+} - X_i^{K^-}}(U_i^{K^+} - U_i^{K^-}) = 0, \quad \omega_i^{k^+} - \omega_i^{k^-} - (\Omega_i^{K^+} - \Omega_i^{K^-}) = 0, \tag{9}$$

where X_i, U_i and Ω_i are, respectively, the positions, displacements and rotations of the reference nodes, the superscript "K^+" denotes reference nodes N1, N2 and N3, and the superscript "K^-" stands for reference node N0. For uniaxial compression along $-\boldsymbol{e}_1$, say, node N0 is fixed and a displacement corresponding to $\varepsilon_1 = -0.001$ is applied at node N1. The reaction force induced in element E01, called ETF1 in ABAQUS, can be substituted into Eq. (5) for F_1, and the axial displacements of elements E02 and E03, called EU1 in ABAQUS, can be inserted into Eqs. (6a,b) for u_2^1 and u_3^1, respectively.

3. Results and discussion

3.1. Size sensitivity

Before proceeding to model 3-D foams having irregular cell shapes and non-uniform SCSAs, an important issue that needs to be resolved is to determine the appropriate number of cells to be included in a specimen and the appropriate number of specimens (S) to be analyzed for each type of foams. Based on a finite element analysis of random heterogeneous materials using representative volume elements (RVEs) of various sizes, Kanit et al. (2003) found that for a given precision the effective elastic properties of the materials can be obtained through using either a large RVE accompanied by a small number of specimens or a small RVE accompanied by a large number of specimens. This indicates that the number of specimens needs to be carefully chosen for accurate predictions. As mentioned earlier, in the current study the number of specimens is initially taken to be 20 (i.e., $S = 20$), which is the same as that used in Li et al. (2005b). Four groups of specimens, each group containing a same number of cells C ($C \in \{8, 27, 64, 125, 216\}$), are considered to determine the appropriate C. For each group, twenty specimens are modeled to obtain the mean values m and standard deviations δ of the effective properties. For all of the four groups of specimens, the shape irregularity amplitude a and the relative density R remain, respectively, to be 0.5 and 0.01, and the strut cross-sectional shape is taken to be Plateau border. The obtained numerical results of E_1, E_2, E_3, G_{12}, G_{23}, G_{31}, ν_{12}, ν_{23} and ν_{31} are graphically shown in Figs. 8–10. To better illustrate these results, the three

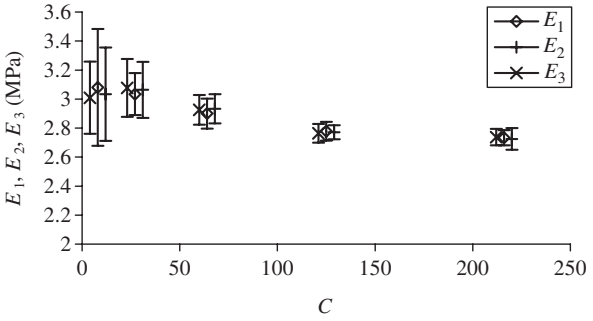

Fig. 8. Young's moduli vs. the number of cells.

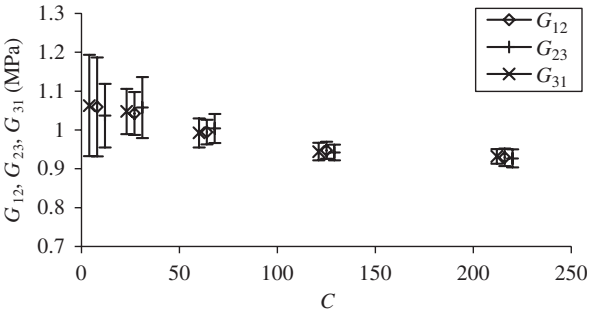

Fig. 9. Shear moduli vs. the number of cells.

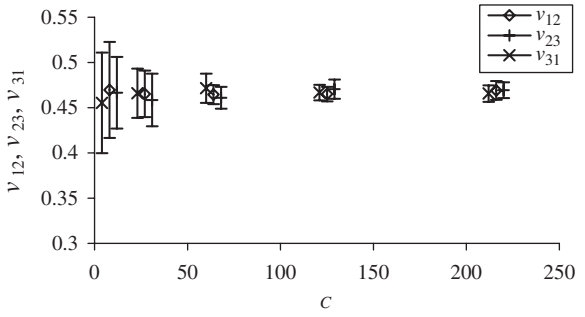

Fig. 10. Poisson's ratios vs. the number of cells.

standard deviation bars of the corresponding properties for each value of C are drawn separately along the C axis, despite the fact that C is the same for all three properties shown in each figure.

From Figs. 8–10 it is seen that as the number of cells (C) increases, the mean values of the effective Young's moduli and the effective shear moduli decrease slightly, while those of the effective Poisson's ratios remain almost the same. The standard deviations (δ) of all the nine properties decrease significantly with the increase of C for $C \leqslant 125$. When $C = 125$, δ is small (no more than 4% of the mean value) for all the nine properties.

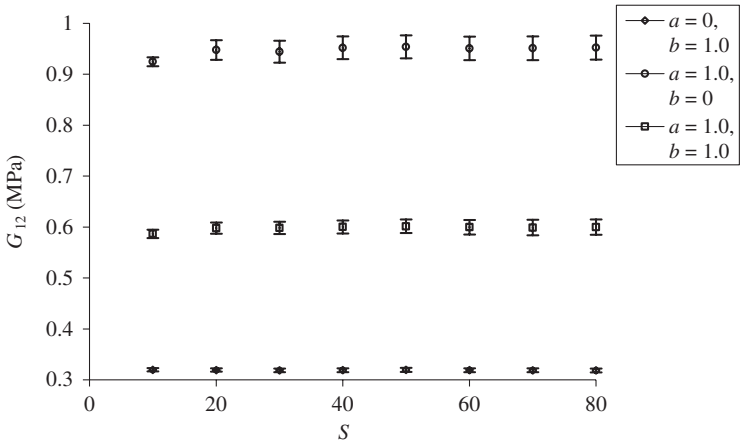

Fig. 11. The shear modulus varying with the number of specimens.

Further increase of C does not result in significant changes in the values of δ, although small fluctuations (reflecting the random nature of the foam structures) are observed. Therefore, $C = 125$ is chosen as the number of cells to be included in each specimen.

In order to evaluate whether the initially chosen number of specimens ($S = 20$) is an appropriate one, finite element analyses are conducted on three types of foams: the completely irregular foams with a uniform SCSA ($a = 1.0$, $b = 0$), the regular foams with completely non-uniform SCSAs ($a = 0$, $b = 1.0$), and the completely irregular foams with completely non-uniform SCSAs ($a = 1.0$, $b = 1.0$). Each specimen contains 125 cells and has a relative density $R = 0.01$. The mean values (m) and standard deviations (δ) of the effective shear modulus G_{12} are obtained for the three types of foams using various values of S ($S \in \{10, 20, 30, 40, 50, 60, 70, 80\}$), which are shown in Fig. 11. It is observed from Fig. 11 that there is a slight increase in the mean values of G_{12} as S increases from 10 to 20, and further increase of S does not lead to any significant changes in the values of m and δ. Hence, the initial choice of $S = 20$ as the number of specimens is appropriate.

3.2. Isotropy of the effective properties

A total of 38 cases, which can be classified as four groups, as listed in Table 1, are analyzed in this study. Controlling parameters include the degree of cell shape irregularity (amplitude a), the degree of SCSA non-uniformity (amplitude b), the relative density (R) and the strut cross-sectional shape. The shapes for the strut cross section examined here include circle, square, equilateral triangle and Plateau border. The effect of these four different strut cross-sectional shapes on the effective elastic properties of perfectly ordered foams was originally studied by Warren and Kraynik (1997). Among these four shapes, Plateau boarder is believed to be closest to actual strut cross-sectional shapes (e.g., Warren and Kraynik, 1997; Li et al., 2003). This is supported by recent experimental observations reported in Sarzynski and Ochoa (2005) and Gong et al. (2005a), whose micrographs showed that the true strut cross-section shape for an open-cell carbon or polymeric foam is indeed closer to Plateau border than to other shapes. Hence, most of the simulations to be presented below are conducted for foams with Plateau border strut cross-sections, as

Table 1
Modeling cases

Group number	Cross-sectional shape	R	a	b	Remarks
1	Plateau border	0.01	0, 0.1, 0.2, 0.3, 0.4, 0.5, 0.8, 1.0	0	Effects of cell shape irregularity
2	Plateau border	0.01	0, 1.0	0, 0.2, 0.5, 0.8, 1.0	Effects of SCSA non-uniformity
3	Plateau border	0.01, 0.06, 0.11, 0.16, 0.22	0, 1.0	0, 1.0	Effects of the relative density
4	Plateau border, equilateral triangle, square, circle	0.01, 0.11	1.0	1.0	Effects of the strut cross-sectional shape

Table 2
Isotropy of elastic properties

Ratio of elastic properties	$m_{\max}$	$m_{\min}$	$\delta_{\max}$
E_1/E_2	1.023677	0.991939	0.065771
E_2/E_3	1.014180	0.986012	0.055143
E_3/E_1	1.010613	0.981335	0.066920
v_{12}/v_{21}	1.023682	0.993173	0.065750
v_{23}/v_{32}	1.014122	0.981473	0.055130
v_{31}/v_{13}	1.010553	0.981386	0.067005
G_{12}/G_{12}^T	1.003098	0.993218	0.022807
G_{23}/G_{23}^T	1.007912	0.996438	0.019437
G_{31}/G_{31}^T	1.008779	0.996548	0.023663

indicated in Table 1. Except for the cases with $a = 0$ and $b = 0$ (i.e., perfect foams) (totaling 5), the mean values and standard deviations of the elastic properties for each case listed in Table 1 are obtained from the results of the finite element analyses performed on twenty specimens. For the former (i.e., perfect foams with different values of R), only one specimen is needed in each case. The maximum and minimum mean values ($m_{\max}$ and $m_{\min}$) and the maximum standard deviations ($\delta_{\max}$) of E_1/E_2, E_2/E_3, E_3/E_1, v_{12}/v_{21}, v_{23}/v_{32} and v_{31}/v_{13} are given in Table 2. In addition, to examine whether the shear relation $G = E/[2(1+v)]$ is satisfied, which is required for material isotropy, the results for $m_{\max}$, $m_{\min}$ and $\delta_{\max}$ of G_{12}/G_{12}^T, G_{23}/G_{23}^T and G_{31}/G_{31}^T are also listed in Table 2, where the values of G_{12}^T, G_{23}^T and G_{31}^T are, respectively, obtained using $G_{12}^T = E_1/[2(1+v_{12})]$, $G_{23}^T = E_2/[2(1+v_{23})]$ and $G_{31}^T = E_3/[2(1+v_{31})]$. An inspection of Table 2 indicates that the extreme mean values of each of the nine ratios are very close to unity, and the maximum standard deviations are all small (less than 7% of the corresponding mean values). Therefore, it can be concluded, as a fairly good approximation, that the elastic response of the foams studied is isotropic regardless of changes in cell shape irregularity, SCSA non-uniformity, relative density and strut cross-sectional shape. Note that Kelvin foams (i.e., perfectly ordered foams with $a = 0$, $b = 0$) are included among these foams for comparison. It is known that Kelvin foams exhibit weak anisotropy (in the form of cubic symmetry) in their

elastic responses (Warren and Kraynik, 1997). Accordingly, only three properties, i.e., E_1, G_{12} and v_{12}, will be discussed in the sequel. Similar trends can be observed for other effective elastic properties.

3.3. Effects of cell shape irregularity

The effects of irregular cell shapes on elastic properties are analyzed for low-density foams having the same relative density (e.g., $R = 0.01$). For each value of a, twenty independent lists of random variables φ_i^k ($i \in \{1, 2, 3\}$; $k \in \{1, \ldots, M\}$) are used to generate twenty foam samples, each of which has a unique arrangement of struts. Finite element analyses are then conducted on the twenty samples, and the mean values and standard deviations of the effective properties, i.e., the Young's moduli, Poisson's ratios and shear moduli, are obtained.

Figs. 12–14 graphically show the predicted values of the Young's modulus E_1, shear modulus G_{12} and Poisson's ratio v_{12} at different values of a. From Figs. 12 and 13, it is observed that, on average, both E_1 and G_{12} increase considerably with a (up to $a = 0.5$) and then stay, respectively, around 2.8 and 0.95 MPa with small variations as a increases further. This implies that foams with $a = 0.5$ may be regarded as highly irregular. Further increase of a (beyond 0.5) can no longer significantly lower the regularity of cell shapes, as noted in Sections 2.1 and 2.2. The mean values of E_1 and G_{12} at $a = 1.0$ are, respectively,

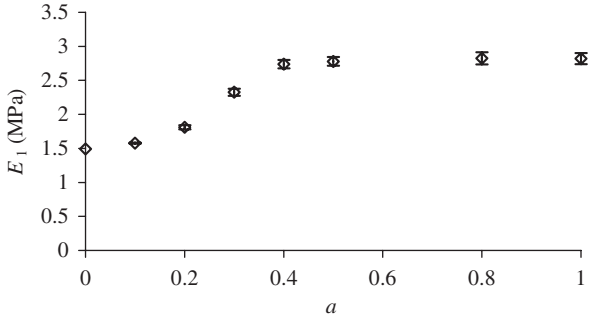

Fig. 12. Effects of cell shape irregularity on the Young's modulus E_1 (with $R = 0.01$).

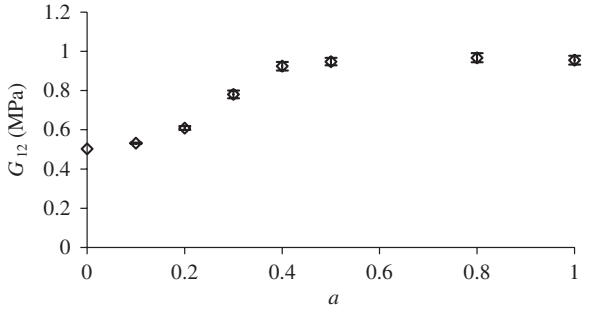

Fig. 13. Effects of cell shape irregularity on the shear modulus G_{12} (with $R = 0.01$).

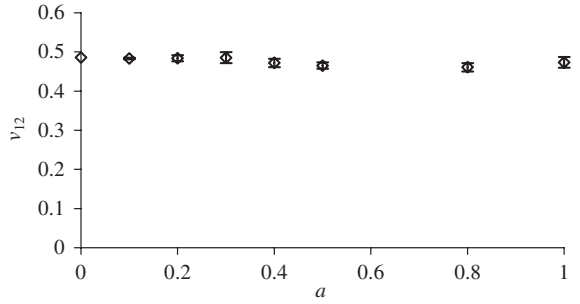

Fig. 14. Effects of cell shape irregularity on the Poisson's ratio v_{12} (with $R = 0.01$).

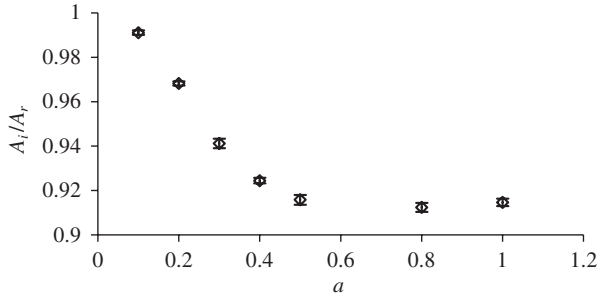

Fig. 15. Effects of cell shape irregularity on the non-dimensional SCSA (with $R = 0.01$).

86.4% and 88.6% larger than their corresponding values at $a = 0$. The regular foam (with $a = 0$) is the softest in terms of the elastic moduli. This conforms to what was observed by Van der Burg et al. (1997). As a increases, the mean values of the Poisson's ratio v_{12}, however, decrease slightly, as shown in Fig. 14. Fig. 15 indicates the reduction of normalized SCSA, A_i/A_r, with the increase of a (up to $a = 0.5$), which undermines the moduli. Here, A_r and A_i are, respectively, the SCSAs of regular and irregular foams. For the same reason as that for the effects of a on the moduli, the mean values of A_i/A_r change insignificantly when $a > 0.5$ (see Sections 2.1 and 2.2). These observations are similar to what was found in Li et al. (2005b) for 2-D imperfect cellular solids. To explore the reason for the strong dependence of the moduli on cell shape irregularity, Van der Burg et al. (1997) visualized the stress distributions in the struts of a foam specimen loaded by uniaxial tension. They found that as the foam becomes less regular, stretching deformations in the struts are fostered, which is similarly observed for imperfect honeycombs by Li et al. (2005b). Van der Burg et al. (1997) further attributed the enhancement in the foam moduli to the appearance of chains of struts with large axial stresses along the loading direction when the cells in the foam get irregular. These chains were believed to transmit the applied load from one cell face to another in the specimen. This stiffening effect substantially outweighs the loss in stiffness caused by the small decrease in the SCSA, thereby leading to a significant increase of the elastic moduli. The dependence of foam moduli on cell shape irregularity observed here is supported by the scatter in the data for moduli of various actual (random) foams with different cell shapes

and sizes obtained through numerous experiments (see Figs. 5.10 and 5.11 in Gibson and Ashby, 1997).

Roberts and Garboczi (2002) analyzed random, isotropic open-cell foams with a roughly uniform cell size. They also used the Voronoi tessellation technique to generate foam models, each containing approximately 125 cells, and applied periodic boundary conditions to each foam specimen in their finite element analyses. Their foam models have shapes similar to the ones generated here with $a = 0.1$ [see Fig. 2(a)]. Based on five specimens, they obtained the mean values of the elastic properties as $E = 2.06244\,\text{MPa}$, $G = 0.70501\,\text{MPa}$ and $v = 0.44$. The Young's modulus and Poisson's ratio of the solid strut material used in their study are, respectively, $E_s = 1\,\text{GPa}$ and $v_s = 0.2$. To compare with their results, finite element simulations of five specimens having the same R, E_s and v_s as theirs are conducted in this study. Each specimen contains 125 cells, as shown in Fig. 2(a), and has a relative density of 0.05. The mean values of the Young's modulus E_1, the shear modulus G_{12} and the Poisson's ratio v_{12} predicted in the current study are, respectively, 2.05136 MPa, 0.71336 MPa and 0.43711, which are very close to the predictions of Roberts and Garboczi (2002) mentioned above.

3.4. Effects of SCSA non-uniformity

For three-dimensional open-cell foams, the influence of SCSA variations on the elastic properties is still unclear. The regular foams with $a = 0$, the irregular foams with $a = 0.3$, and the completely random foams with $a = 1.0$, all having non-uniform SCSAs, are therefore analyzed here. Four values of the SCSA non-uniformity amplitude, i.e., $b = 0.2$, 0.5, 0.8 and 1.0, are used for each of the three values of a. When $b = 1.0$, SCSA variations are completely random. For each pair of a and b, twenty foam samples are modeled using independent lists of random variables φ_i^k $(i \in \{1,2,3\}; k \in \{1,\ldots,M\})$ and ψ_j $(j \in \{1,\ldots,N\})$. The relative density remains to be 0.01 for the samples analyzed here, and more samples with different values of R will be discussed in Section 3.5.

The predicted values of the effective Young's modulus E_1, shear modulus G_{12} and Poisson's ratio v_{12} at various values of b are shown in Figs. 16–18. Figs. 16 and 17 indicate that for all the three values of a considered the elastic moduli E_1 and G_{12} significantly decrease as b increases. For the regular foams ($a = 0$), both E_1 and G_{12} are reduced by 36% as b changes from 0 to 1.0, while the relative reduction is 37% for fully irregular foams with $a = 1.0$ and 36% for the irregular foams with $a = 0.3$. The Poisson's ratio v_{12},

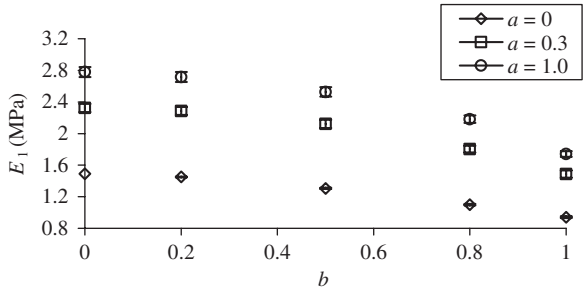

Fig. 16. Effects of SCSA variations on the Young's modulus E_1 (with $R = 0.01$).

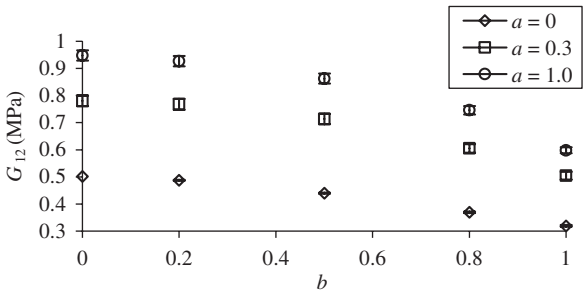

Fig. 17. Effects of SCSA variations on the shear modulus G_{12} (with $R = 0.01$).

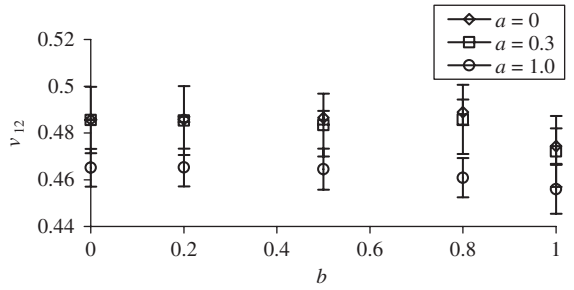

Fig. 18. Effects of SCSA variations on the Poisson's ratio v_{12} (with $R = 0.01$).

however, is negligibly influenced in each case by the values of b, as shown in Fig. 18. An inspection of Figs. 16–18 also reveals that for each value of b the elastic moduli are the highest for the completely irregular foam with $a = 1.0$, the second highest for the irregular foam with $a = 0.3$, and the lowest for the regular foam with $a = 0$, while the Poisson's ratio is slightly lower for the irregular foam with $a = 1.0$ than those for the irregular foam with $a = 0.3$ and the regular foam with $a = 0$. These agree with what has been observed from Figs. 12–14.

Moreover, it can be seen from Figs. 16–18 that the differences between the mean values of the elastic moduli for each two of the three types of foams with $a = 1.0$, 0.3 and 0 are insignificantly affected by varying b. This implies that the effect of the interaction between the cell shape and SCSA variations on the elastic moduli of each foam is weak. When these two variations are very small (i.e., $a \ll 1$, $b \ll 1$), the weak interaction observed here can be analytically shown to be true for any such imperfect foam with a given value of R (see Appendix).

A further examination of Figs. 16 and 17 shows that the elastic moduli are affected more by the cell shape irregularity than by the SCSA non-uniformity. This follows from the fact that the elastic moduli for the case with $a = 1.0$, $b = 1.0$ are larger than the corresponding ones for the case with $a = 0$, $b = 0$ (i.e., foams without imperfections), even though the two elastic moduli are both found to increase as a increases (for fixed values of b) and to decrease with the increase of b (for fixed values of a), as discussed earlier. The trend observed above is based on low-density foams (with $R = 0.01$ here) and differs from that exhibited by foams with large values of R, which will be discussed next.

3.5. Effects of the relative density

Figs. 19–21 graphically show the results of the effective Young's modulus E_1, shear modulus G_{12} and Poisson's ratio v_{12} as a function of the relative density for four types of foams: the regular foams with a uniform SCSA ($a = 0$, $b = 0$), the completely irregular foams with a uniform SCSA ($a = 1.0$, $b = 0$), the regular foams with completely

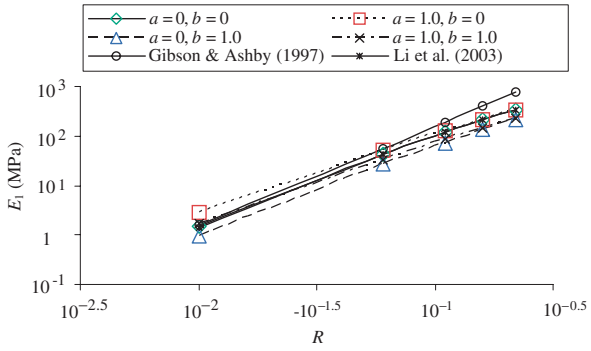

Fig. 19. Effects of the relative density on the Young's modulus E_1 (in logarithmic scales).

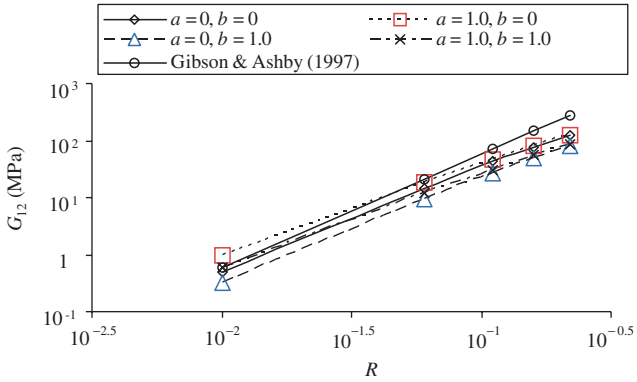

Fig. 20. Effects of the relative density on the shear modulus G_{12} (in logarithmic scales).

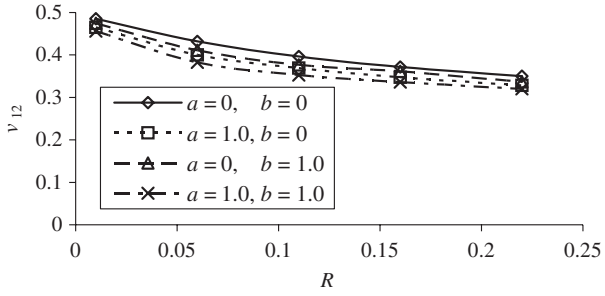

Fig. 21. Effects of the relative density on the Poisson's ratio v_{12}.

non-uniform SCSAs ($a = 0$, $b = 1.0$), and the completely irregular foams with completely non-uniform SCSAs ($a = 1.0$, $b = 1.0$). The variation of the effective Young's modulus (E_1) with the relative density (R) predicted using the unit cell models of Gibson and Ashby (1997) and Li et al. (2003) is also illustrated in Figs. 19 and 20, which are log–log plots, for comparison. In calculating E_1 using the formulas derived in Li et al. (2003) [see Eqs. (25) and (28) there], the effective cross-sectional area of the unit cell (A^*) is taken to be $7L^2$, which is the area projected by the tetrakaidecahedral unit cell onto the xy-plane (see Fig. 3 in Li et al., 2003). For the foams with a uniform SCSA (i.e., $b = 0$), the relative density (R) depends on the SCSA, as dictated by Eq. (2). The relative density of the irregular foams with $b \neq 0$ depends not only on the SCSAs but also on cell shapes, as governed by Eqs. (2)–(4). Five relative densities, i.e., 0.01, 0.06, 0.11, 0.16 and 0.22, are used for each type of the foams listed above. For the perfect foams (i.e., $a = 0$, $b = 0$) only one model is needed for each density. For the remaining three types of foams with cell shape and/or SCSA imperfections, twenty models are constructed for each density except for the case with $R = 0.01$, which has been dealt with in the previous simulations. The statistical distributions of φ_i^k ($i \in \{1, 2, 3\}$; $k \in \{1, \ldots, M\}$) and ψ_j ($j \in \{1, \ldots, N\}$) for the models with $R = 0.06$, 0.11, 0.16 and 0.22 remain the same as those for the models with $R = 0.01$.

As shown in Figs. 19 and 20, E_1 and G_{12} for each of the four types of foams considered increase with the relative density. For the perfect foams ($a = 0$, $b = 0$) with the Plateau border strut cross-section, Fig. 19 shows that the values of the effective Young's modulus (E_1) predicted by the unit cell model developed in Li et al. (2003) are in very good agreement with the finite element results. It is also noted from Figs. 19 and 20 that at low relative densities the elastic moduli (i.e., E_1 and G_{12}) predicted by the current finite element model agree well with those estimated by the unit cell model of Gibson and Ashby (1997), which says $E_m/E_s = K_m R^2$, with the constant K_m determined from curve fitting experimental data. Here, E_m stands for E_1 or G_{12}. However, as the relative density becomes large, the finite element model tends to underestimate the elastic moduli. This arises from the simplifying assumption that the cross-sectional area is uniform along the length of each strut, which works well only for foams having low relative densities (Kraynik, 2003; Gong et al., 2005a). For a given value of R, the fact that the values of E_1 and G_{12} for the perfect foam (with $a = 0$, $b = 0$) are smaller than those for the foams with $a = 1.0$ and $b = 0$ and larger than those for the foams with $a = 0$ and $b = 1.0$ indicates that the elastic moduli (E_1 and G_{12}) are enhanced by the cell shape irregularity but undermined by the SCSA non-uniformity. This agrees with the observation made earlier based on Figs. 12, 13, 16 and 17 for foams with $R = 0.01$. Smaller values of E_1 and G_{12} for the imperfect foams with $a = 1.0$ and $b = 1.0$ than those for the perfect foams (with $a = 0$, $b = 0$) observed here from Figs. 19 and 20 implies that the stiffness-strengthening effect caused by the cell shape irregularity is less pronounced than the stiffness-weakening effect due to the SCSA non-uniformity when R is large. This is the same as that for 2-D imperfect honeycombs found in Li et al. (2005b).

Fig. 21 illustrates the relations between the Poisson's ratio v_{12} and the relative density R. For all of the four types of foams, v_{12} decreases moderately with the increase of R. It is seen that for various values of R considered, both types of imperfections slightly reduce v_{12}, and for imperfect foams the influence of a is larger than that of b when $a = b$ ($= 1.0$).

In order to further explore the effects of the relative density (R) on the behavior of foams having the two co-existing imperfections, the relative differences between the elastic properties of the imperfect foams and those of the perfect foams (with $a = 0$, $b = 0$) are

calculated and examined here. Let

$$e_Q = \frac{Q^r - Q^p}{Q^p}, \tag{10}$$

where e_Q is the relative difference, Q denotes the elastic property (E_1 or G_{12}), and the superscripts r and p stand for, respectively, the random and perfect foams. The numerical results for e_Q as a function of R are illustrated in Figs. 22 and 23.

It is observed from Figs. 22 and 23 that when R increases, the magnitudes of the relative differences, e_Q, induced solely by the presence of irregular cell shapes (i.e., $a = 1.0$, $b = 0$) decrease, while those caused purely by the presence of non-uniform SCSAs (i.e., $a = 0$, $b = 1.0$) remain almost unchanged. Here, a positive value of e_Q represents an increase in the modulus and a negative value of e_Q indicates a decrease in the modulus, both relative to the modulus of the perfect foam having the same value of R. A further examination of Figs. 22 and 23 reveals that when R is small, the increase in the moduli due to the appearance of irregular cell shapes (i.e., $a = 0.3$, 0.5, 1.0) is larger than the decrease in the moduli caused by the presence of non-uniform SCSAs (i.e., $b = 0.3$, 0.5, 1.0). When R becomes large, however, the effects of the SCSA non-uniformity on the elastic moduli are more significant than those of the cell shape irregularity. As a result, e_Q is negative for the

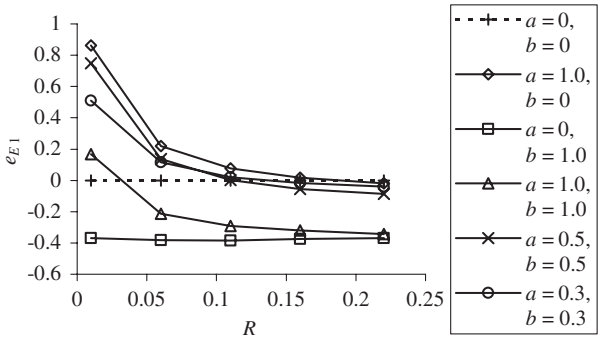

Fig. 22. Differences in the Young's modulus varying with the relative density.

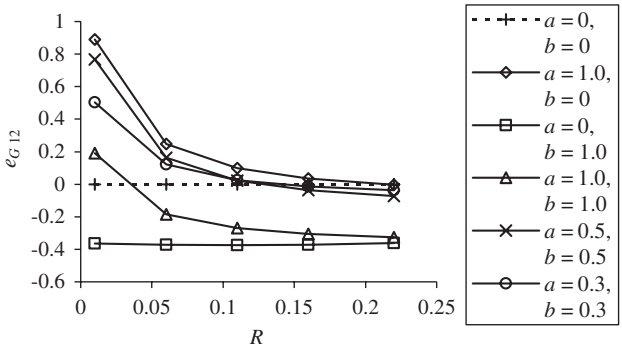

Fig. 23. Differences in the shear modulus varying with the relative density.

foams with the two co-existing imperfections (i.e., $a = b = 0.3$, 0.5, 1.0 here) when R is large, as illustrated in Figs. 22 and 23. This indicates that for large relative densities the elastic moduli of these imperfect foams are smaller than those of the perfect foams (i.e., $a = 0$, $b = 0$). These observations support and enhance those made earlier based on Figs. 16 and 17 for foams with $R = 0.01$ and on Figs. 19 and 20 for foams with various values of R.

3.6. Effects of strut cross-sectional shapes

The effects of strut cross-sectional shapes are studied using completely irregular foams with completely non-uniform SCSAs (i.e., $a = 1.0$, $b = 1.0$). Four cross sections, i.e., Plateau border (PB), equilateral triangle (ET), square (SQ) and circle (CR), and two relative densities, i.e., 0.01 and 0.11, are used. The predicted mean values of normalized elastic properties Q^{cs}/Q^{PB}, where the superscript "cs" refers to PB, ET, SQ or CR, at various values of R are graphically illustrated in Fig. 24. To better view the datum points for the cross-section PB, some of them (e.g., points for G_{12} at $R = 0.11$, ν_{12} at $R = 0.11$, G_{12} at $R = 0.01$, and E_1 at $R = 0.11$) are intentionally shown at positions other than the common (single) point where they are all supposed to be. It is seen from Fig. 24 that for a given value of R, E_1 and G_{12} are the highest for the Plateau border strut cross section, followed by the equilateral triangle, square and circular strut cross sections. The order of influence of the strut cross-sectional shape on ν_{12} is opposite to that on the moduli. These conform to what was found in Warren and Kraynik (1997) and Li et al. (2003) for perfectly ordered foams using unit cell based models. An inspection of Fig. 24 also indicates that the values of Q^{cs}/Q^{PB} are larger for a higher value of R. This implies that as R increases, the differences in the elastic moduli (E_1 and G_{12}) resulting from the use of different strut cross sections are reduced, while those in the Poisson's ratio (ν_{12}) increase. In addition, a further examination of Fig. 24 shows that for both values of R considered, the elastic moduli are more sensitive to the strut cross-sectional shape than the Poisson's ratio is. This is reflected by the fact that the maximum relative difference in E_1 and G_{12} caused by utilizing different strut cross sections (approximately 20%) is larger than that in ν_{12} (8%) for $R = 0.11$. The disparity is even larger for lower values of R: the maximum relative differences in the elastic moduli and the Poisson's ratio are, respectively, 21% and 6% when $R = 0.01$.

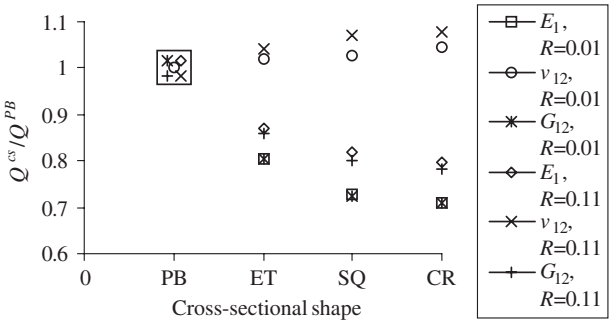

Fig. 24. Effects of strut cross-sectional shapes on normalized elastic properties.

4. Summary

The effects of cell shape and strut cross-sectional area (SCSA) imperfections on the elastic properties of 3-D open-cell cellular solids (foams) are studied using the Voronoi tessellation technique and the finite element (FE) method. Voronoi diagrams with different degrees of cell shape irregularity (amplitude a) are produced by perturbing regularly packed seeds. Perturbations are then introduced to the uniform cross-sectional area of the struts to generate a uniform distribution of SCSAs with different degrees of non-uniformity (amplitude b). Twenty FE models are constructed, based on the Voronoi diagrams for twenty foam samples having the same pair of a and b, to obtain the mean values and standard deviations of the elastic properties.

Based on the simulation results and analyses presented, the following conclusions can be drawn:

(1) The elastic response of foams with cell shape and SCSA imperfections appears to be isotropic regardless of changes in the cell shape irregularity (amplitude a), the SCSA non-uniformity (amplitude b), the relative density (R) and the strut cross-sectional shape. It is known that perfectly ordered Kelvin foams ($a = 0$) exhibit weak anisotropy (in the form of cubic symmetry) in their elastic responses (Warren and Kraynik, 1997). The random orientation of the struts in a randomly structured foam ($a \neq 0$) is the main reason for the isotropic elastic behavior displayed by imperfect foams.

(2) For low-density random foams with struts of a uniform cross-sectional area, as the cell shapes become more irregular, on average, the elastic moduli increase considerably, while the Poisson's ratios decrease slightly.

(3) For regular foams, the increase in the SCSA non-uniformity substantially reduces the elastic moduli but has little influence on the Poisson's ratios.

(4) When irregular cell shapes and non-uniform SCSAs co-exist in a foam, the effect of the interaction between the two types of imperfections on the elastic properties appears to be weak. For low-density foams, when the degree of irregularity and the degree of non-uniformity are equal, the stiffness gain resulting from the appearance of irregular cells is more than the stiffness loss due to the perturbation to the uniform SCSA. As the relative density (R) increases, however, this order of influence is reversed. Consequently, the elastic moduli of the foams with the two co-existing imperfections are lower than those of the perfect foams when R becomes large.

(5) When the relative density increases, the elastic moduli of imperfect foams increase remarkably, while the Poisson's ratios decrease moderately.

(6) The strut cross-sectional shape has a significant effect on the elastic properties of imperfect foams. At a given relative density, the highest moduli and lowest Poisson's ratios are obtained for the Plateau border cross section, followed by the equilateral triangle, square and circular strut cross-sections. Also, elastic moduli appear to be more sensitive to the strut cross-sectional shape than Poisson's ratios do. This supplements the similar findings by Warren and Kraynik (1997) based on their analysis of perfectly ordered foams.

Acknowledgments

The work reported here was partially funded by a grant from the AFOSR and by a contract from L & L Products. These supports are gratefully acknowledged. The public access to the Qhull program initially made available by the Geometry Center at the

University of Minnesota–Twin Cities is also greatly appreciated. In addition, the authors wish to thank Professor K. Bhattacharya and two anonymous reviewers for their helpful comments on an earlier version of the paper.

Appendix

When the relative density R is specified and the strut cross-sectional shape is known, the elastic modulus E_m (representing E_1, E_2 or G_{12}) of an imperfect foam having irregular cell shapes (described by amplitude a) and non-uniform strut cross-sectional areas (described by amplitude b) can be expressed as a function of a and b, i.e., $E_m = E_m(a,b)$. Consider a neighborhood of the point $(a,b) = (0,0)$, which represents the perfect foam with the specified value of R and the given strut cross-sectional shape. Suppose that the function $E_m(a, b)$ is infinitely differentiable with respect to a and b in the neighborhood. Then, it can be expanded about $(a,b) = (0,0)$ as a power series of the following form:

$$E_m = E_m^o + \sum_{i,j=1}^{\infty} \beta_{ij} a^i b^j, \tag{A.1}$$

where $E_m^o \equiv E_m(0,\ 0)$ is the elastic modulus of the perfect foam, and β_{ij} are the expansion coefficients. If the degrees of cell shape irregularity and strut cross-sectional area non-uniformity are very small such that $a \ll 1$ and $b \ll 1$, then this power series of infinitely many terms may be approximated by a finite number of leading terms (up to the fifth order here) as

$$\begin{aligned} E_m = E_m^o &+ \beta_{10}a + \beta_{20}a^2 + \beta_{30}a^3 + \beta_{40}a^4 + \beta_{01}b + \beta_{02}b^2 + \beta_{03}b^3 + \beta_{04}b^4 + \beta_{11}ab \\ &+ \beta_{12}ab^2 + \beta_{13}ab^3 + \beta_{21}a^2b + \beta_{22}a^2b^2 + \beta_{31}a^3b + o(a,b)^5. \end{aligned} \tag{A.2}$$

Since a ($\in [0,1]$) and b ($\in [0,1]$) are, respectively, introduced in Eqs. (1) and (3) through a product with the random variables $\varphi_i \in [-1,1]$ and $\psi_j \in [-1,1]$, they could have been redefined to range over $[-1,\ 1]$ without changing the obtained results for the elastic properties. Mathematically, this requires $E_m(a,b) = E_m(-a,b) = E_m(a,-b)$. Then, it follows from Eq. (A.2) and these necessary conditions that the coefficients β_{ij} of all terms odd in a or b in the series should be zero. Hence, the truncated series given in Eq. (A.2) becomes

$$E_m = E_m^o + \beta_{20}a^2 + \beta_{40}a^4 + \beta_{02}b^2 + \beta_{04}b^4 + \beta_{22}a^2b^2 + o(a,b)^6. \tag{A.3}$$

This shows that there is only one mixed term (i.e., $\beta_{22}a^2b^2$) in the power series up to the fifth order. Therefore, the effect of the interaction between the two imperfections (as measured respectively by a and b) on E_m is indeed weak, thereby confirming what is revealed by the numerical results presented in the paper for the more general case of imperfect foams with small or large variations in cell shape and strut cross-sectional area (i.e., with both a and b varying in the full range of [0, 1], as opposed to the case with $a \ll 1$ and $b \ll 1$ discussed here).

The power series based technique presented above was first used by Grenestedt and Tanaka (1999) in analyzing closed-cell foams with irregular cell shapes, where E_m depends on the cell shape irregularity amplitude [i.e., $E_m = E_m(a)$] for a given value of R. The feasibility of using the technique to analyze honeycombs with two co-existing cell shape and cell wall thickness imperfections was demonstrated by Grenestedt (2003).

References

Bart-Smith, H., Bastawros, A.-F., Mumm, D.R., Evans, A.G., Sypeck, D.J., Wadley, H.N.G., 1998. Compressive deformation and yielding mechanisms in cellular Al alloys determined using X-ray tomography and surface strain mapping. Acta Mater. 46, 3583–3592.

Gibson, L.J., Ashby, M.F., 1997. Cellular Solids: Structures and Properties, second ed. Cambridge University Press, Cambridge.

Glaessgen, E.H., Phillips, D.R., Iesulauro, E., Saether, E., Piascik, R.S., 2003. A multiscale approach to modeling fracture in metallic materials containing nonmetallic inclusions. AIAA 2003-1616. American Institute of Aeronautics and Astronautics, Reston, VA.

Gong, L., Kyriakides, S., Jang, W.-Y., 2005a. Compressive response of open-cell foams. Part I: morphology and elastic properties. Int. J. Solids Struc. 42, 1355–1379.

Gong, L., Kyriakides, S., Triantafyllidis, N., 2005b. On the stability of Kelvin cell foams under compressive loads. J. Mech. Phys. Solids 53, 771–794.

Grenestedt, J.L., 1998. Influence of wavy imperfections in cell walls on elastic stiffness of cellular solids. J. Mech. Phys. Solids 46, 29–50.

Grenestedt, J. L., 2003. Personal communications.

Grenestedt, J.L., Bassinet, F., 2000. Influence of cell wall thickness variations on elastic stiffness of closed-cell cellular solids. Int. J. Mech. Sci. 42, 1327–1338.

Grenestedt, J.L., Tanaka, K., 1999. Influence of cell shape variations on elastic stiffness of closed cell cellular solids. Script. Mater. 40, 71–77.

Hibbitt, Karlsson, Sorensen, Inc., 2002. ABAQUS Theory and User's Manuals, Version 6.3. Hibbitt, Karlsson and Sorensen, Inc., Pawtucket, RI.

Kanit, T., Forest, S., Galliet, I., Mounoury, V., Jeulin, D., 2003. Determination of the size of the representative volume element for random composites: statistical and numerical approach. Int. J. Solids Struc. 40, 3647–3679.

Kraynik, A.M., 2003. Foam structure: from soap froth to solid foams. MRS Bull. 28, 275–278.

Kraynik, A.M., Reinelt, D.A., van Swol, F., 2003. Structure of random monodisperse foam. Phys. Rev. E 67, 031403-1-11.

Kraynik, A.M., Reinelt, D.A., van Swol, F., 2004. Structure of random foam. Phys. Rev. Lett. 93, 208301-1-4.

Laroussi, M., Sab, K., Alaoui, A., 2002. Foam mechanics: nonlinear response of an elastic 3D-periodic microstructure. Int. J. Solids Struc. 39, 3599–3623.

Li, K., Gao, X.-L., Roy, A.K., 2003. Micromechanics model for three-dimensional open-cell foams using a tetrakaidecahedral unit cell and Castigliano's second theorem. Compos. Sci. Tech. 63, 1769–1781.

Li, K., Gao, X.-L., Roy, A.K., 2005a. Micromechanical analysis of three-dimensional open-cell foams using the matrix method for spatial frames. Composites: Part B 36, 249–262.

Li, K., Gao, X.-L., Subhash, G., 2005b. Effects of cell shape and cell wall thickness variations on the elastic properties of two-dimensional cellular solids. Int. J. Solids Struc. 42, 1777–1795.

Matzke, E.B., 1946. The three-dimensional shape of bubbles in foam—an analysis of the role of the surface forces in three-dimensional cell shape determination. Amer. J. Botany 33, 58–80.

Nygards, M., Gudmundson, P., 2002. Three-dimensional periodic Voronoi grain models and micromechanical FE-simulations of a two-phase steel. Comp. Mat. Sci. 24, 513–519.

Roberts, A.P., Garboczi, E.J., 2001. Elastic moduli of model random three-dimensional closed-cell cellular solids. Acta Mater. 49, 189–197.

Roberts, A.P., Garboczi, E.J., 2002. Elastic properties of model random three-dimensional open-cell solids. J. Mech. Phys. Solids 50, 33–55.

Sarzynski, M.D., Ochoa, O.O., 2005. Carbon foam core composite sandwich beams: flexure response. J. Compos. Mater. 39, 1067–1080.

Silva, M.J., Gibson, L.J., 1997. The effects of non-periodic microstructure and defects on the compressive strength of two-dimensional cellular solids. Int. J. Mech. Sci. 39, 549–563.

Silva, M.J., Hayes, W.C., Gibson, L.J., 1995. The effects of non-periodic microstructure on the elastic properties of two-dimensional cellular solids. Int. J. Mech. Sci. 37, 1161–1177.

Simone, A.E., Gibson, L.J., 1998a. Effects of solid distribution on the stiffness and strength of metallic foams. Acta Mater. 46, 2139–2150.

Simone, A.E., Gibson, L.J., 1998b. The effects of cell face curvature and corrugations on the stiffness and strength of metallic foams. Acta Mater. 46, 3929–3935.

Thompson, W. (Lord Kelvin), 1887. On the division of space with minimal partitional area. Philos. Mag. 24, 503–514.

Van der Burg, M.W.D., Shulmeister, V., Van der Geissen, E., Marissen, R., 1997. On the linear elastic properties of regular and random open-cell foam models. J. Cell. Plastics 33, 31–54.

Warren, W.E., Kraynik, A.M., 1997. Linear elastic behavior of a low-density Kelvin foam with open cells. ASME J. Appl. Mech. 64, 787–794.

Weaire, D., Fortes, M.A., 1994. Stress and strain in liquid and solid foams. Adv. Phys. 43, 685–738.

Zhou, J., Mercer, C., Soboyejo, W.O., 2002. An investigation of the microstructure and strength of open-cell 6101 aluminum foams. Metallurg. Mater. Trans. A 33, 1413–1427.

Zhu, H.X., Knott, J.F., Mills, N.J., 1997. Analysis of the elastic properties of open-cell foams with tetrakaidecahedral cells. J. Mech. Phys. Solids 45, 319–343.